Acta Cryst. (1998). A**54**, 1006–1013

Thermal Diffuse Scattering in Angular-Dispersive Neutron Diffraction

N. C. Popa[a] and B. T. M. Willis[b]*

[a]*Institute of Materials Physics, PO Box MG-7, Bucharest, Romania, and* [b]*Chemical Crystallography Laboratory, University of Oxford, 9 Parks Road, Oxford OX1 3PD, England. E-mail: bertram.willis@chemcryst.ox.ac.uk*

(*Received 25 March 1998; accepted 6 May 1998*)

Abstract

The theoretical treatment of one-phonon thermal diffuse scattering (TDS) in single-crystal neutron diffraction at fixed incident wavelength is reanalysed in the light of the analysis given by Popa & Willis [*Acta Cryst.* (1994), A**50**, 57–63; *Acta Cryst.* (1997), A**53**, 537–545] for the time-of-flight method. Isotropic propagation of sound with different velocities for the longitudinal and transverse modes is assumed. As in time-of-flight diffraction, there exists, for certain scanning variables, a forbidden range in the one-phonon TDS of slower-than-sound neutrons, and this permits the determination of the sound velocity in the crystal. A fast algorithm is given for the TDS correction of neutron diffraction data collected at a fixed wavelength: this algorithm is similar to that reported earlier for the time-of-flight case.

1. Introduction

The theoretical treatment of one-phonon thermal diffuse scattering (TDS) that is close to the Bragg reflection has been treated many years ago by Willis (1970) and by Cooper (1971) for the angular-dispersive (AD) method of neutron diffraction. The principal conclusion from these papers was that the TDS of faster-than-sound neutrons is similar to that measured in X-ray diffraction but is essentially different for slower-than-sound neutrons. The main concept used to explain this difference and to calculate the TDS correction of the Bragg peaks was the 'scattering surface', defined as the locus of the end points of the wave vectors $\mathbf{q}$ of the phonons contributing to the scattering. The topology of the scattering surface is dependent on $\beta = c/v_n$, the ratio between the sound and the neutron velocities. For $\beta < 1$, the scattering surface is a hyperboloid of two sheets, one sheet corresponding to phonon creation and the other to phonon annihilation. On the other hand, for $\beta > 1$, the scattering surface is an ellipsoid. Any point on this ellipsoid corresponds to either phonon creation or phonon annihilation, according to whether the scanning parameter is on one side or the other of the Bragg peak. By using a simplified one-velocity model, in which all acoustic phonons have the same velocity, Cooper (1971) calculated the TDS correction of the Bragg peaks for three scanning types: the crystal scan, the θ–2θ scan (or $\omega/2\theta$ scan) and the radial scan. However, the results of Cooper must be considered to be only partially valid because, for $\beta > 1$, the scattering surface is not always an ellipsoid. In this paper, we shall reconsider Cooper's results and extend them to a fourth scanning type known as the detector scan. All four scans through the reciprocal-lattice point are illustrated in Fig. 1. The figure is drawn assuming that the Bragg reflection occurs at a sharply defined point in reciprocal space and that the detector accepts radiation at a sharply defined scattering angle 2θ.

2. One-phonon scattering surfaces

Let us denote by $\mathbf{Q}$ the wavevector transfer between the incident and scattered neutrons, by $\mathbf{Q}_e$ the wavevector transfer of elastically scattered neutrons, and by $h\omega$ the energy transfer. As shown by Popa & Willis (1994) (hereafter PW1†), the three-dimensional scattering surface defined above and denoted by SS3 is the intersection of a scattering surface SS4 in four-dimensional space $(\mathbf{Q}_e, \hbar\omega)$ with a plane P in the space $\mathbf{Q}_e$ ($\hbar$ is Planck's constant h divided by 2π). SS4 is obtained by projecting into the $(\mathbf{Q}_e, \hbar\omega)$ space, from $(\mathbf{Q}, \hbar\omega)$ space, the intersection points between the integration curves specific to the diffraction method and the dispersion surface of the acoustic phonons. The crossing plane P is normal to the diffraction plane (*i.e.* the plane containing the incident and Bragg scattered beams) and it contains the scanning direction. The resultant SS3 has different topologies in three intervals of β: $(0, \beta_v)$, (β_v, β_μ) and (β_μ, ∞). In the first interval, SS3 is a hyperboloid of two sheets which is defined for any value of the scanning parameter. In the second interval, SS3 is also a hyperboloid of two sheets but there exists a finite range in the scanning parameter for which TDS is forbidden. In the third interval of β, SS3 is an ellipsoid, and TDS is then permitted in a finite range of the scanning parameter and forbidden outside this range. In other words, the TDS differential cross section is defined in any range of $\mathbf{Q}_e$ if $\beta \leq \beta_v$, but only in a certain domain of $\mathbf{Q}_e$ if $\beta > \beta_v$,

† There are two minor errors in PW1 which do not affect the remaining analysis in that paper. In the definition of $\mathbf{Q}$ on p. 58 of PW1, ψ should be replaced by $\psi^{1/2}$ and, in equation (11) on p. 60, φ should be replaced by $\varphi^{1/2}$.

ISSN 0108-7673

this domain being dependent on the magnitude of β. Finally, the value of β_μ depends on the type of scan.

Although PW1 refers specifically to the time-of-flight (TOF) diffraction method, all the statements above are valid for AD diffraction and it is only the particular values of β_ν and β_μ that are specific to the diffraction method. For the TOF method, β_ν depends on the diffractometer setting (*i.e.* flight paths and scattering angle). For the AD method, as will be seen below and in agreement with Willis (1970) and Cooper (1971), β_ν is always 1. However, β_μ is 1 only for the 2θ scan (or detector scan); for other scanning types, $\beta_\mu > 1$, which necessitates the recalculation of the TDS correction factor in the AD method. In this paper, an algorithm for the TDS correction is given, which is similar to that reported by Popa & Willis (1997) (hereafter PW2) for the TOF method. As in PW2, an isotropic model with two sound velocities is used. These velocities may or may not be known beforehand: in the latter case, the algorithm can be incorporated in the structure refinement program by treating the sound velocities as refinable parameters.

A second reason for re-analysing the problem of TDS in AD diffraction is to demonstrate the possibility of measuring by this diffraction method the sound velocity in the crystal. Willis *et al.* (1986) have determined the sound velocity in pyrolitic graphite by using the TOF diffraction method. Similar measurements on calcium fluoride and barium fluoride were reported by Carlile & Willis (1989), who determined the width of the TOF interval which is forbidden for TDS and which occurs when β is in the range (β_ν, β_μ). By choosing the diffractometer setting in the AD method to have $\beta_\mu \to \infty$, a very large range of sound velocity can be measured and, as will be shown below, this condition can be realised by using the radial scan.

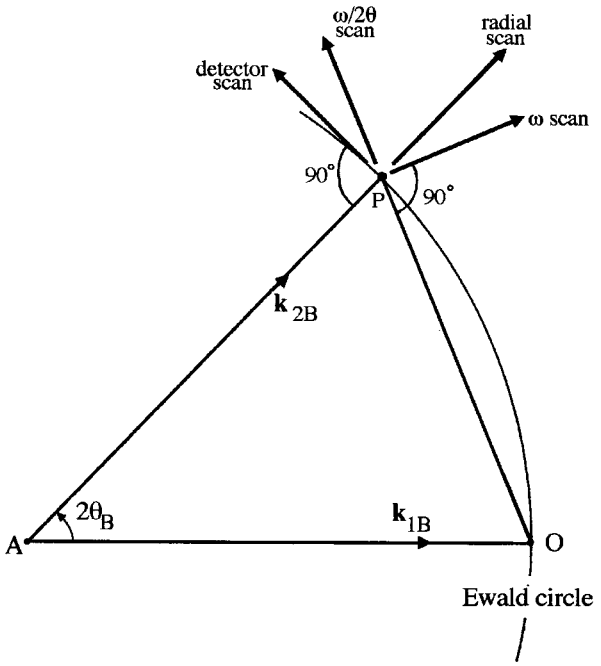

Fig. 1. Diagram in reciprocal space illustrating the four types of scan through a Bragg reflection. (O is the origin of reciprocal space and A is the centre of the Ewald sphere.) For the more general scans considered in the text, the scanning directions are the same but the scans do not necessarily pass through the lattice point.

3. Differential cross section for thermal diffuse scattering in the AD neutron diffraction method

In the AD diffraction method, the TDS differential cross section is derived by using the same approximations as for the TOF method. Thus, only the scattering from low-energy acoustic phonons is taken into account. These phonons are associated with longitudinal or transverse modes, with group velocities c_1 and c_2, respectively. The high-temperature approximation (whereby the mode energy is equal to $K_B T$ where K_B is the Boltzmann constant) is used and the instrumental resolution is ignored. Details of the consequences of these approximations can be found in PW1. The flow of calculation is similar, but there are some specific differences.

We start from the same double differential cross section [equation (8) in PW1], performing the sum over $\mathbf{q}$ and then integrating over the energy of the scattered neutron E_2, instead of over the energy E_1 of the incident neutron. The dimensionless variables x, y, γ, δ are also introduced but the significance of x and y are different. In this paper, $x = (k_2 - k_B)/k_B$, where $k_2 = |\mathbf{k}_2|$ and $k_B = |\mathbf{k}_{2B}|$, with $\mathbf{k}_2$ the wavevector of neutrons scattered in a general direction and $\mathbf{k}_{2B}$ the wavevector of the Bragg scattered neutrons. The incident neutrons, of wavevector $\mathbf{k}_1$, have a fixed wavelength and $\mathbf{k}_1 \approx \mathbf{k}_{1B}$ because resolution is ignored. y is the offset angle of the crystal from the Bragg angle θ_B, *i.e.* $y = \theta - \theta_B$. The variables γ and δ have the same significance as in PW1, δ being the angle between $\mathbf{k}_2$ and its projection in the diffraction plane and γ being the angle between this projection and $\mathbf{k}_{2B}$ (see Fig. 2).

The scattering geometry is illustrated in Fig. 2. $2\pi\mathbf{H}_B$ is the reciprocal-lattice vector to the lattice point hkl at P, and $2\pi\mathbf{H}$ is the same vector after rotation of the crystal about an axis normal to the diffraction plane. The vectors $\mathbf{k}_2$, $\mathbf{Q}$ and $\mathbf{q}$ are shown projected in this plane.

The variables x, y, γ, δ define the coordinates of points in the spaces $(\mathbf{Q}, \hbar\omega)$, $(\mathbf{Q}_e, \hbar\omega)$ and $\mathbf{Q}$. Let us choose an orthogonal coordinate system $(\mathbf{I}, \mathbf{J}, \mathbf{L})$ where

$$\mathbf{I} = (\mathbf{k}_{1B} + \mathbf{k}_{2B})/|\mathbf{k}_{1B} + \mathbf{k}_{2B}|,$$
$$\mathbf{J} = (\mathbf{k}_{2B} - \mathbf{k}_{1B})/|\mathbf{k}_{2B} - \mathbf{k}_{1B}|,$$
$$\mathbf{L} = \mathbf{I} \times \mathbf{J}.$$

For phonon scattering in the neighbourhood of the Bragg peak, $x, y, \gamma, \delta \ll 1$ and we can write

$$\mathbf{Q} = 2\pi\mathbf{H}_B + k_B(x\cos\theta_B - \gamma\sin\theta_B)\mathbf{I} + k_B(x\sin\theta_B + \gamma\cos\theta_B)\mathbf{J} + k_B\delta\mathbf{L} \quad (1a)$$

$$2\pi\mathbf{H} = 2\pi\mathbf{H}_B - 2k_B(\sin\theta_B)y\mathbf{I} \quad (1b)$$

$$\mathbf{Q}_e = \mathbf{Q}(x = 0) \quad (1c)$$

and

$$\omega = \hbar(k_B)^2 x/m_n, \quad (1d)$$

where m_n is the neutron mass.

In some scanning procedures used in the AD diffraction method, the crystal and detector are moved together. In this case, y and γ are dependent variables. To have independent variables, we introduce γ' in place of γ by the following relation:

$$\gamma = ry + \gamma'. \quad (2)$$

By choosing r appropriately and varying y or γ', any scanning type, conventional or otherwise, can be carried out. Thus,

(a) $r = 0$, γ' constant, y varying, defines the ω or crystal scan (crystal moving);

(b) $r = 0$, y constant, γ' varying, defines the 2θ or detector scan (detector moving);

(c) $r = 2$, γ' constant, y varying, defines an $\omega/2\theta$ scan (both crystal and detector moving);

(d) $r = 2\sin^2\theta_B$, γ' constant, y varying, defines a radial scan (both crystal and detector moving).

As will be seen in the next section, the radial scan gives the possibility of measuring *any* sound velocity greater than the neutron velocity.

Returning now to the calculation of the differential cross section, we need to use the momentum and energy conservation laws:

$$\mathbf{q} = \mathbf{Q} - 2\pi\mathbf{H}, \quad (3a)$$

$$\omega = -\varepsilon\omega_j(\mathbf{q}). \quad (3b)$$

Here, $\omega_j(\mathbf{q})$ is the phonon frequency for the branch j, ε is $+1$ for phonon creation and -1 for phonon annihilation. In the isotropic approximation $\omega_j(\mathbf{q}) = c_j q$, where c_j is the sound velocity. If this expression is inserted into (3b) and (1d) is used, the phonon wave number becomes

$$q = -\varepsilon k_B x/\beta_j. \quad (4)$$

Now, by equalizing q^2 from (3a) and (4) and taking into account (1a) and (2), we obtain the following equation for the variable x (index j omitted):

$$(\beta^2 - 1)x^2 + 2\beta^2 Mx + \beta^2 N^2 = 0, \quad (5)$$

where M and N^2 are defined by

$$M = y\sin 2\theta_B, \quad (6a)$$

$$N^2 = (\gamma' - by)^2 + M^2 + \delta^2 \quad (6b)$$

with b given by equation (9a) below. Equation (5) represents the scattering surface SS4. It is similar, but not identical, to equation (16) in PW1 for time-of-flight diffraction. The solutions of (5) give the energies and wave vectors of those acoustic phonons that contribute to the TDS and are measured simultaneously with the Bragg scattering at a given point of the space $\mathbf{Q}_e$, near to $2\pi\mathbf{H}_B$. The solutions are:

$$x_{1,2} = \beta(-\beta M \pm \Delta^{1/2})/(\beta^2 - 1), \quad (7a, b)$$

where $\Delta = \beta^2 M^2 - (\beta^2 - 1)N^2$.

For $\beta \leq 1$, the solutions (7a) exist at any point (y, γ', δ). One solution is positive and corresponds to phonon annihilation, the other is negative and corresponds to phonon creation. For $\beta > 1$, the solutions exist only for the points (y, γ', δ) inside the cone of two sheets $\Delta(y, \gamma', \delta) = 0$. Both take the sign of $-M$, corresponding to phonon creation for $y > 0$ and to phonon annihilation for $y < 0$. Outside the cone the solutions $x_{1,2}$ do not exist and there is no TDS.

The cone equation is

$$\Delta = (1 - \beta^2)\gamma'^2 + a^2(1 - \beta^2/\beta_\mu^2)y^2 - 2b(1 - \beta^2)\gamma' y + (1 - \beta^2)\delta^2 = 0, \quad (8)$$

where

$$b = 2\sin^2\theta_B - r, \quad (9a)$$

$$a^2 = b^2 + \sin^2 2\theta_B \quad (9b)$$

$$\beta_\mu^2 = a^2/b^2. \quad (9c)$$

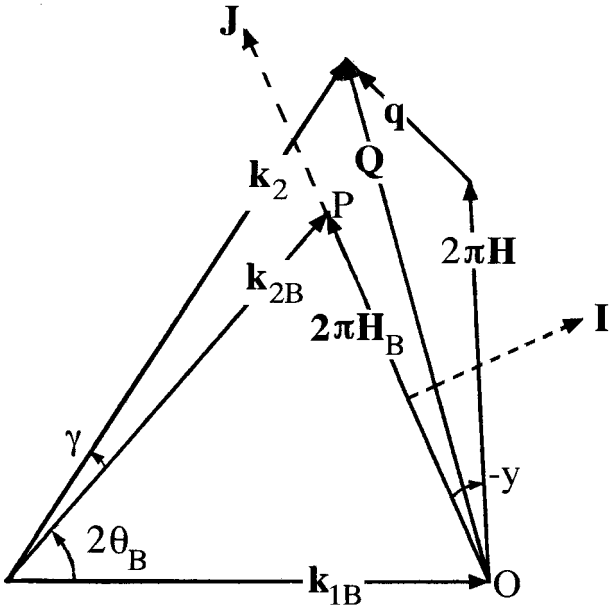

Fig. 2. Scattering geometry in reciprocal space showing definition of angles γ, y, which are assumed small.

The cone axis lies in the plane (y, γ') and its slope has the sign of the parameter b defined by (9a). When β increases from 1 to ∞, the cone angle decreases from π to zero. There is a particular value $\beta = \beta_\mu$ with $\beta > 1$, which is defined by (9c) and for which the axis y lies on the cone surface; for $1 < \beta < \beta_\mu$, this axis is inside the cone and, for $\beta_\mu < \beta < \infty$, it is outside. An exception is the case of the radial scan, for which $b = 0$; then $\beta_\mu = \infty$ and the axis y is the cone axis for any value of $\beta > 1$.

All these statements are readily proved by writing down the solutions of equation (8). This is performed in Appendix A where the solutions are denoted by $y_\pm(\gamma', \delta)$ if the equation is solved in the variable y and by $\gamma'_\pm(y, \delta)$ if the equation is solved in γ'. The curves $y = y_\pm(\gamma', \delta)$ or $\gamma' = \gamma'_\pm(y, \delta)$ for a given value of δ represent the cross sections of the cone with a plane parallel to the (y, γ') plane. This is a two-branch hyperbola degenerating into its asymptotic lines for $\delta = 0$. Fig. 3 illustrates typical cases drawn for $\theta_B = 30°$. The dashed curves show the cross section of the cone with the plane $\delta = 0.02$ and the full lines the cross section with $\delta = 0$. Figs. 3(a) and (b) both apply to the crystal scan and the detector scan, and Figs. 3(e) and (f) to the $\omega/2\theta$ scan. The value of β is in the range $(1, \beta_\mu)$ for Figs. 3(a) and (e) and in the range (β_μ, ∞) for Figs. 3(b) and (f). Figs. 3(c) and (d) apply to the radial scan (with $\beta_\mu = \infty$) for two different values of $\beta > 1$ but taking $b = 0$.

Having found the domain of definition in the space $\mathbf{Q}_e$, we can now write down the expression for the TDS differential cross section:

$$\mathrm{d}\sigma_{\mathrm{TDS}}/\mathrm{d}\Omega(\mathbf{Q}_e) = (4\pi/3)(V/v_c)|F|^2 \sin^2\theta_B \times \sum_{j=1}^{2} j(K_B T/M_c c_j^2) S_j(y, \gamma', \delta). \quad (10)$$

Here, V is the sample volume, v_c and M_c the unit-cell volume and mass, F the structure factor for Bragg scattering, K_B the Bolzmann constant and T the sample temperature. If the index j (which comes from its dependence on β_j) is ignored, the function $S(y, \gamma', \delta)$ in (10) is

$$S(y, \gamma', \delta) = \begin{cases} 1/\pi N^2 \\ \quad \text{for } \beta \le 1 \text{ and for any point } (y, \gamma', \delta) \\ (1/\pi N^2)(\beta|M|/\Delta^{1/2}) \\ \quad \text{for } \beta > 1 \text{ and for } (y, \gamma', \delta) \text{ inside the cone.} \end{cases} \quad (11)$$

At the point $\mathbf{Q}_e = 2\pi\mathbf{H}_B$, the function $S(y, \gamma', \delta)$ has an infinite integrable singularity, and if $\beta > 1$ this function has the same kind of singularity on the surface of its domain of definition. The TDS differential cross section for AD diffraction, as given by (10) and (11), has the same form as that derived in PW1 for the TOF method, but the functions M, N and Δ are different.

4. The measurement of sound velocity by the AD method of neutron diffraction

If slower-than-sound neutrons are used, the existence of discontinuities on the surface of the definition domain of $S(y, \gamma', \delta)$ can be exploited to measure the sound velocity in the crystal. To see how this can be performed, let us first integrate $S(y, \gamma', \delta)$ over the parameter δ, which represents the vertical divergence of the scattered beam from the horizontal diffraction plane. If the range of divergence is $(-\delta_0, \delta_0)$, one obtains for $\beta \le 1$:

$$S(y, \gamma') = A^{-1}(2/\pi) \arctan(\delta_0 A^{-1}), \quad (12)$$

where the function A is

$$A^2(y, \gamma') = N^2 - \delta^2 = (\gamma' - by)^2 + y^2 \sin^2 2\theta_B. \quad (13)$$

For $\beta > 1$, we have:

$$S(y, \gamma') = \begin{cases} A^{-1}(2/\pi) \arctan(\delta_0 \beta |M| A^{-1} \Delta^{-1/2}) \\ \quad \text{for } (y, \gamma') \subset D(\delta_0) \\ A^{-1} \quad \text{for } (y, \gamma') \subset D(0) - D(\delta_0) \\ 0 \quad \text{otherwise,} \end{cases} \quad (14)$$

where $D(\delta)$ denotes the domain of points (y, γ') lying outside the branches of the hyperbola in Fig. 3. Equation (14) shows that $S(y, \gamma')$ has a discontinuity of amplitude $1/A$ on the borders of its definition domain $D(0)$, which are the lines $\gamma' = \gamma'_\pm(y, 0)$. Fig. 4 shows some typical dependencies of $S(y, \gamma')$ on the variable y for a set of discrete values of γ'. Figs. 4(a), (b), (c) have been drawn by using the same parameters r, θ_B, β and $\delta_0 = \delta$ as those used for Figs. 1(a), (d), (f), respectively. If $1 < \beta < \beta_\mu$, there exists a range $y_-(\gamma', \delta_0) \le y \le y_+(\gamma', \delta_0)$ where TDS is forbidden, whereas TDS is permitted in this range but forbidden outside if $\beta_\mu < \beta < \infty$. At the limits of this range in y, $S(y, \gamma')$ has a sharp cut off.

To measure a sound velocity greater than the neutron velocity, we need to set a high thin slit in the front of the detector and to perform a scan far enough from the point $(y, \gamma') = (0, 0)$ so as not to record the Bragg intensity. If the $\omega/2\theta$ scan is used, $\beta_\mu = 1/\cos\theta_B$. This is the same expression as for TOF diffraction, which is not surprising as in both cases the scanning takes place along a direction parallel to the reciprocal-lattice vector $\mathbf{H}_B$. The width of the forbidden (f) or permitted (p) range for TDS is then

$$\Delta y_{f,p} = |\gamma'| \tan\theta_B (\beta^2 - 1)^{1/2} / |1 - \beta^2 \cos^2\theta_B|.$$

For the ω scan, $\beta_\mu = 1/\sin\theta_B$ and the width of the forbidden or permitted range for TDS is

$$\Delta y_{f,p} = |\gamma'| \cot\theta_B (\beta^2 - 1)^{1/2} / |1 - \beta^2 \sin^2\theta_B|.$$

For the detector scan there is a permitted range for any $\beta > 1$ (see Figs. 3*a*, *b*) whose width is

$$\Delta\gamma_p = 2|y| \sin 2\theta_B/(\beta^2 - 1)^{1/2}.$$

Finally, for the radial scan, $\beta_\mu = \infty$ and there exists a forbidden range of width

$$\Delta y_f = |\gamma'|(\beta^2 - 1)^{1/2}/\sin 2\theta_B.$$

The detector scan in the AD method was used many years ago by Shirane *et al.* (1965) and by Alperin *et al.* (1967) to measure the magnon dispersion relation in iron and magnetite, respectively. Hitherto, the TOF

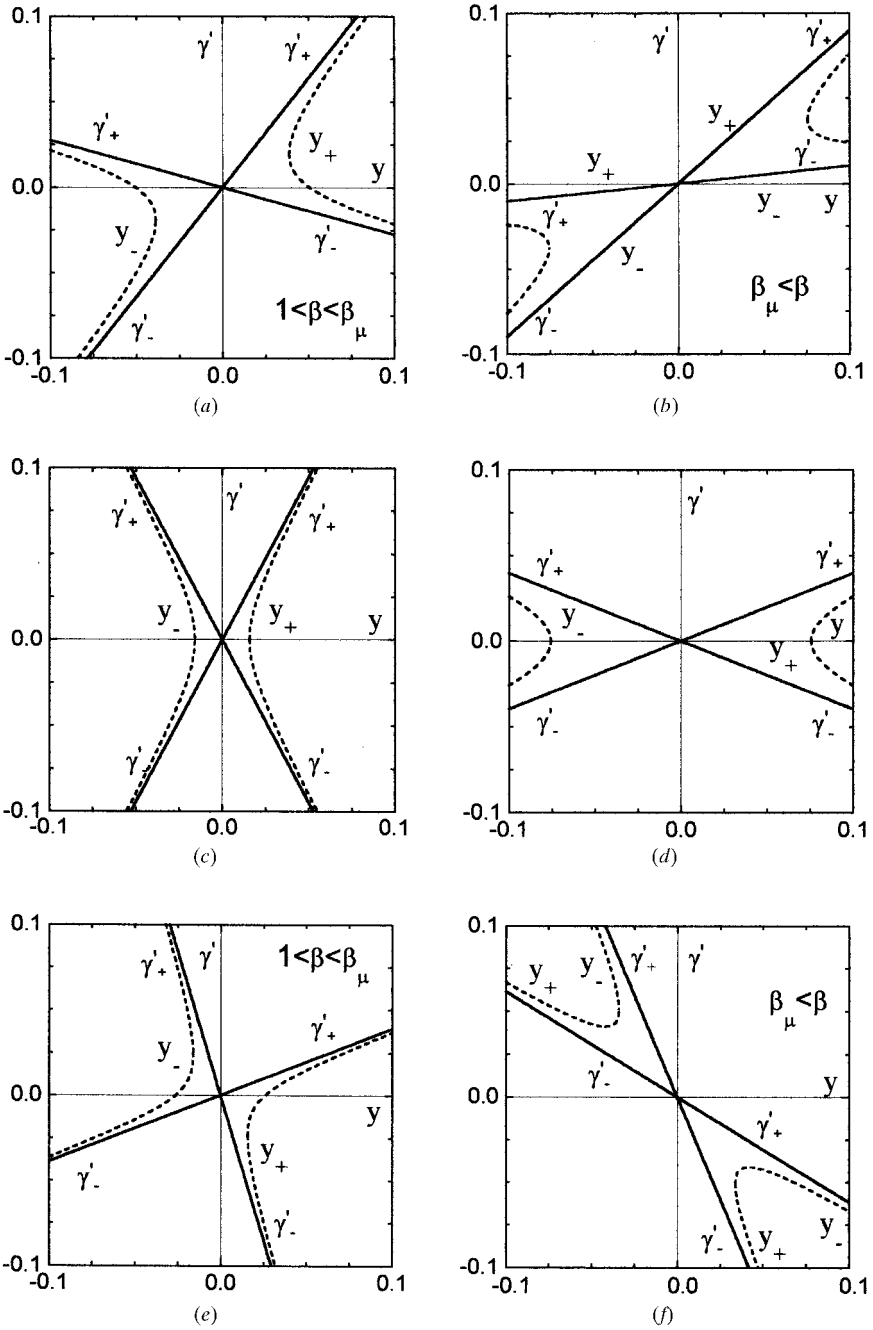

Fig. 3. For $\beta > 1$, the function $S(y, \gamma', \delta)$ is defined only inside a cone of two sheets. The dashed curves show the cross section of the cone with the plane $\delta = 0.02$ and the thick lines the cross section with $\delta = 0$. (*a*) and (*b*) correspond to both the ω scan and the 2θ scan, (*c*) and (*d*) to the radial scan, and (*e*) and (*f*) to the $\omega/2\theta$ scan. θ_B is 30° and the values of r, β_μ and β are respectively: (*a*) 0, 2, 1.5; (*b*) 0, 2, 2.4; (*c*) 0.5, ∞, 1.1; (*d*) 0.5, ∞, 2.4; (*e*) 2, $2/3^{1/2}$, 1.1; (*f*) 0.5, $2/3^{1/2}$, 1.4.

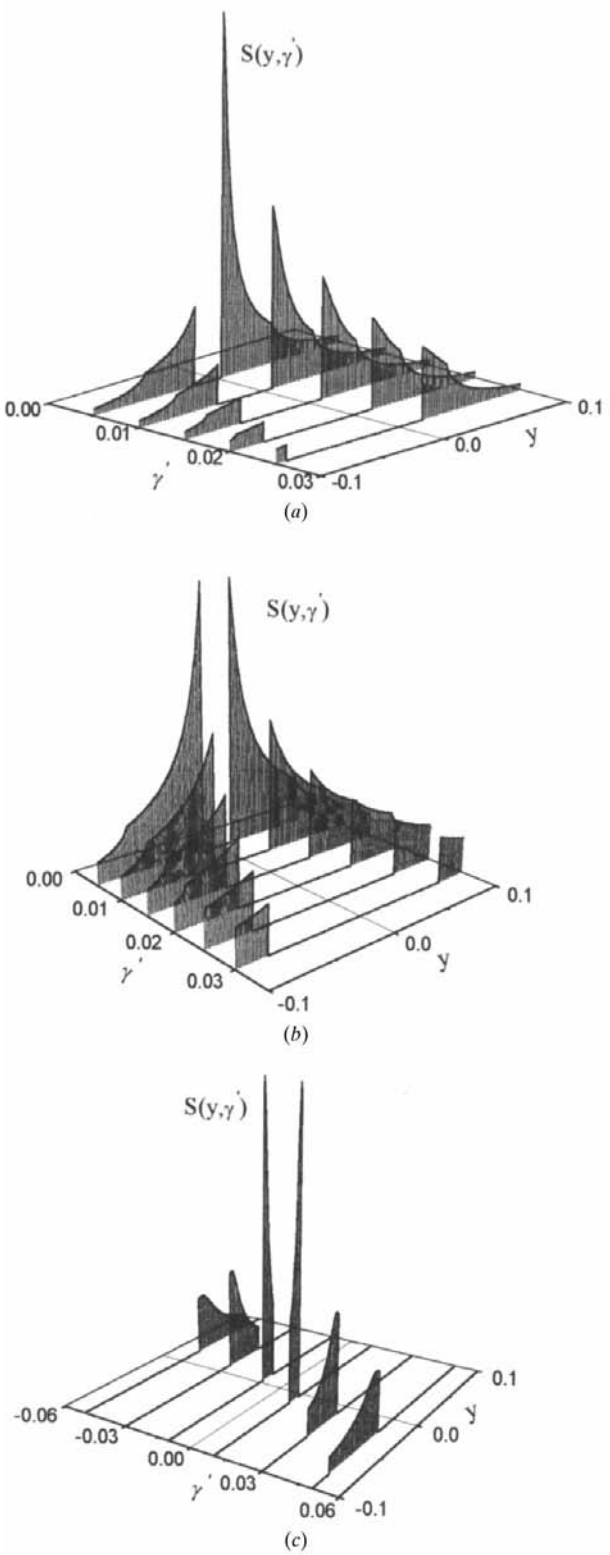

Fig. 4. The dependence of $S(y, \gamma')$ on the variable y for various discrete values of γ'. The figure was drawn for $\theta_B = 30°$, $\delta_0 = 0.02$. The values of r and β in (a), (b) and (c) are the same as in Figs. 3(a), (d) and (f), respectively.

method only has been used for studying acoustic phonons: by Willis *et al.* (1986) to measure the sound velocity in pyrolitic graphite and by Carlile & Willis (1989) to determine the sound velocity in calcium and barium fluorides. These authors measured the width of the forbidden range in time-of-flight diffraction patterns. As shown in this paper, such a forbidden range appears also in the AD method, and this range can be observed for any sound velocity exceeding the neutron velocity by employing the radial scan. The best choice of scan is the one offering the sharpest intensity cut off, and this requires, in turn, an evaluation of the instrumental resolution function.

5. The TDS correction factor

By using (10), one obtains the TDS correction factor of the Bragg peak (see PW2) for the AD method of neutron diffraction:

$$\alpha = (8\pi/3)(v_c/\lambda_B^3)\sin^3\theta_B\cos\theta_B \times \sum_{j=1}^{2} j(K_B T/M_c c_j^2)\tau(\beta_j, \theta_B, y_0, \gamma_0, \delta_0). \quad (15)$$

Here $(2y_0, 2\gamma_0, 2\delta_0)$ is the window in the space (y, γ', δ) containing the entire Bragg peak and τ is given by the following expressions:

$$\tau = 2[S_0 - S(y_0)], \quad (16a)$$

$$S_0 = \int_0^{y_0} \mathrm{d}y\, S(y), \quad (16b)$$

$$S(y) = \int_{-\gamma_0}^{\gamma_0} \mathrm{d}\gamma'\, S(y, \gamma'). \quad (16c)$$

As in PW2, to calculate (16c) we split $S(y, \gamma')$ given by equations (12)–(14) into two terms: $S(y, \gamma') = S_\infty(y, \gamma') - S_\delta(y, \gamma')$. The function $S_\infty(y, \gamma')$, which is the limit of $S(y, \gamma')$ for $\delta_0 \to \infty$, can be integrated analytically over γ'. The result is two terms, the first one of the form $-\ln(y)$ with an infinite singularity at $y = 0$ which can be integrated analytically once (16b) is calculated, and the second one which can be integrated numerically. The function $S_\delta(y, \gamma')$ can also be integrated numerically. As we have shown in PW2, a sufficiently good precision is obtained by using a Gauss quadrature formula with four nodes for a single integral. With this small number of integration nodes, τ can be calculated using a fast routine, which can then be incorporated in a structural refinement program with the sound velocities c_1, c_2 treated as refinable parameters if these are not known beforehand. (This possibility was demonstrated in PW2 using a simulated set of diffraction data.) The algorithm for calculating τ is given in Appendix B for any scanning procedure involving crystal rotation.

Table 1. *Expressions for $S_\infty(y)$*

y range	$0 < y < y_{10}$	$y_{10} < y < y_{20}$	$y_{20} < y < \infty$
$0 < \beta \le 1$	$-2\ln y + R(y) + R(-y)$		
$1 < \beta < \beta_\mu$	R_0	$-\ln y + R(sy) + R_0/2$	$-2\ln y + R(y) + R(-y)$
$\beta = \beta_\mu$	R_0	$-\ln y + R(sy) + R_0/2$ ($y_{20} = \infty$)	
$\beta_\mu < \beta < \infty$	R_0	$-\ln y + R(sy) + R_0/2$	0

A routine has been written in Fortran which applies only to the conventional scanning types, the ω scan and the $\omega/2\theta$ scan. The size of this routine is much reduced by observing that $\tau(\beta, \theta_B, y_0, \gamma_0, \delta_0)$ for the $\omega/2\theta$ scan is equal to $\tau(\beta, \pi/2 - \theta_B, y_0, \gamma_0, \delta_0)$ for the ω scan. Some examples obtained with this routine of the dependence of τ on β are given in Fig. 5. As for TOF diffraction, under certain conditions there is a limiting value β_m beyond which the TDS correction is zero. This condition is given in Appendix *C*.

APPENDIX *A*
Roots of the equation $\Delta(\mathbf{y}, \gamma', \delta) = 0$

Solved in γ' the roots are

$$\gamma'_{+s}(y, \delta) = sP/(\beta^2 - 1),$$
$$\gamma'_{-s}(y, \delta) = s[a^2(\beta^2/\beta_\mu^2 - 1)y^2 + (\beta^2 - 1)\delta^2]/P,$$

where $s = \text{sign}(by)$ and

$$P = |by|(\beta^2 - 1) + \{(\beta^2 - 1)[y^2 \sin^2 2\theta_B - (\beta^2 - 1)\delta^2]\}^{1/2}.$$

Solving for y and denoting $\text{sign}(b\gamma')$ now by s we have:

$$y_{+s}(\gamma', \delta) = s(\beta^2 - 1)(\gamma'^2 + \delta^2)/Q,$$
$$y_{-s}(\gamma', \delta) = sQ/[a^2(\beta^2/\beta_\mu^2 - 1)],$$

where

$$Q = |b\gamma'|(\beta^2 - 1) + \{(\beta^2 - 1)[\gamma'^2 \sin^2 2\theta_B - a^2(\beta^2/\beta_\mu^2 - 1)\delta^2]\}^{1/2}.$$

For $b = 0$, we have

$$\gamma'_\pm(y, \delta) = \pm[y^2 \sin^2 2\theta_B - (\beta^2 - 1)\delta^2]^{1/2}/(\beta^2 - 1)^{1/2}$$

and

$$y_\pm(\gamma', \delta) = \pm[(\beta^2 - 1)(\gamma'^2 + \delta^2)]^{1/2}/\sin 2\theta_B.$$

APPENDIX *B*
The algorithm for calculating factor τ

In this Appendix, we denote $\text{sign}(b)$ by s. We start from

$$S(y, \gamma') = S_\infty(y, \gamma') - S_\delta(y, \gamma'),$$

where

$$S_\infty(y, \gamma') = A^{-1} \tag{17}$$

and

$$S_\delta(y, \gamma') = \begin{cases} A^{-1}[1 - (2/\pi)\arctan(\delta_0 A^{-1})] & \text{for } \beta \le 1 \\ A^{-1}[1 - (2/\pi)\arctan(\delta_0 \beta |M| A^{-1} \Delta^{-1/2})] & \text{for } \beta > 1 \end{cases} \tag{18}$$

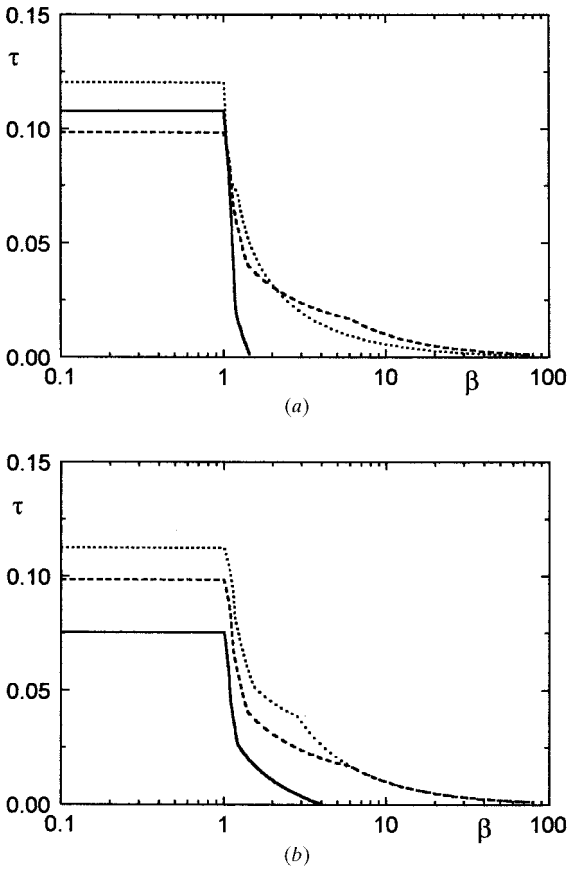

Fig. 5. The parameter τ as a function of β for $\gamma_0 = 0.025$ and $\delta_0 = 0.03$. In (*a*), $y_0 = 0.03$; $\theta_B = 20°$ (full curve), $\theta_B = 45°$ (long-dashed curve) and $\theta_B = 70°$ (short-dashed curve). In (*b*), $\theta_B = 45°$; $y_0 = 0.02$ (full curve), $y_0 = 0.03$ (long-dashed curve) and $y_0 = 0.04$ (short-dashed curve). The curves apply to the ω scan, or $\pi/2$ *minus* these angles for the $\omega/2\theta$ scan.

and where M, A are given by (6*a*) and (13), respectively. Both $S_\infty(y, \gamma')$ and $S_\delta(y, \gamma')$ are defined at any point (y, γ') if $\beta \leq 1$. For $\beta > 1$, $S_\infty(y, \gamma')$ is defined only on $D(0)$ and $S_\delta(y, \gamma')$ only on $D(\delta_0)$.

As was shown in PW2, (17) can be integrated analytically over γ' resulting in $S_\infty(y)$. This function is given by different expressions in different ranges of β and y. If we use the definitions

$$y_{10} = \min[|y_+(\gamma_0, 0)|, |y_-(\gamma_0, 0)|],$$
$$y_{20} = \max[|y_+(\gamma_0, 0)|, |y_-(\gamma_0, 0)|],$$
$$R_0 = \ln[(\beta + 1)/(\beta - 1)]$$
$$R(y) = \ln\{[(\gamma_0 - by) + A(y, \gamma_0)]/\sin 2\theta_B\},$$

the expressions for $S_\infty(y)$ are shown in Table 1.

$S_\delta(y)$ can only be obtained from (18) by numerical integration over γ'. In different β and y ranges, $S_\delta(y)$ is equal to zero or to one of the following functions:

$$T_0(y) = \int_{-\gamma_0}^{\gamma_0} d\gamma' S_\delta(y, \gamma'), \quad T(y) = \int_{\gamma'_-(y,\delta_0)}^{\gamma'_+(y,\delta_0)} d\gamma' S_\delta(y, \gamma'),$$

$$T_+(y) = \int_{\gamma'_-(y,\delta_0)}^{\gamma_0} d\gamma' S_\delta(y, \gamma'), \quad T_-(y) = \int_{-\gamma_0}^{\gamma'_+(y,\delta_0)} d\gamma' S_\delta(y, \gamma').$$

We also need to define

$$y_1 = \min[|y_+(\gamma_0, \delta_0)|, |y_-(\gamma_0, \delta_0)|],$$
$$y_2 = \max[|y_+(\gamma_0, \delta_0)|, |y_-(\gamma_0, \delta_0)|],$$
$$y_* = \delta_0(\beta^2 - 1)^{1/2}/\sin 2\theta_B,$$
$$\gamma'_* = by_*$$
$$\beta_\delta = \beta_\mu[1 + \gamma_0^2 \sin^2 2\theta_B/(a^2\delta_0^2)]^{1/2}.$$

Now we can write down the corresponding table for $S_\delta(y)$ (Table 2). In this table, $\{0;T(y)\}$ corresponds to $\{|\gamma'_*| \geq \gamma_0;\ |\gamma'_*| < \gamma_0\}$.

It is a trivial matter for the reader to write down the explicit expressions of the integrals (16*b*) of $S_\infty(y)$ and $S_\delta(y)$.

Table 2. *Expressions for $S_\delta(y)$*

y range	$0 < y < y_*$	$y_* < y < y_1$	$y_1 < y < y_2$	$y_2 < y < \infty$
$0 < \beta \leq 1$	$T_0(y)$			
$1 < \beta < \beta_\mu$	0	$\{0;T(y)\}$	$T_s(y)$	$T_0(y)$
$\beta = \beta_\mu$	0	$\{0;T(y)\}$	$T_s(y)$ $(y_2 = \infty)$	
$\beta_\mu < \beta < \beta_\delta$	0	$\{0;T(y)\}$	$T_s(y)$	0
$\beta_\delta < \beta < \infty$	0			

APPENDIX *C*
The limiting value of β for a zero TDS correction

There are two conditions for a limiting value β_m beyond which the TDS correction is zero: $y_0 \leq y_{10}$ and $y_0 \leq y_*$. The first condition is fulfilled only when $\gamma_0 > y_0|b|$. In this case, the two conditions give, respectively,

$$\beta_{1m} = [1 + y_0^2 \sin^2 2\theta_B/(\gamma_0 - y_0|b|)^2]^{1/2},$$
$$\beta_{2m} = (1 + y_0^2 \sin^2 2\theta_B/\delta_0^2)^{1/2}$$

and then $\beta_m = \max(\beta_{1m}, \beta_{2m})$. But if $\gamma_0 \leq y_0|b|$ then $\beta_m = \infty$.

This work was supported in part by a Collaborative Research Grant awarded by NATO.

References

Alperin, H. A., Steinsvoll, O., Nathans, R. & Shirane, G. (1967). *Phys. Rev.* **154**, 508–514.
Carlile, C. J. & Willis, B. T. M. (1989). *Acta Cryst.* A**45**, 708–715.
Cooper, M. J. (1971). *Acta Cryst.* A**27**, 148–157.
Popa, N. C. & Willis, B. T. M. (1994). *Acta Cryst.* A**50**, 57–63.
Popa, N. C. & Willis, B. T. M. (1997). *Acta Cryst.* A**53**, 537–545.
Shirane, G., Nathans, R., Steinsvoll, O., Alperin, H. A. & Pickart, S. J. (1965). *Phys. Rev. Lett.* **15**, 146–148.
Willis, B. T. M. (1970). *Acta Cryst.* A**26**, 396–401.
Willis, B. T. M., Carlile, C. J., Ward, R. C., David, W. I. F. & Johnson, M. W. (1986). *Europhys. Lett.* **2**, 767–774.